Oecologia (2006) 149:221–232
DOI 10.1007/s00442-006-0444-x

PLANT ANIMAL INTERACTIONS

Comparison of photosynthetic damage from arthropod herbivory and pathogen infection in understory hardwood saplings

Mihai Aldea · Jason G. Hamilton · Joseph P. Resti · Arthur R. Zangerl · May R. Berenbaum · Thomas D. Frank · Evan H. DeLucia

Received: 4 October 2005 / Accepted: 20 April 2006 / Published online: 7 June 2006

Abstract Arthropods and pathogens damage leaves in natural ecosystems and may reduce photosynthesis at some distance away from directly injured tissue. We quantified the indirect effects of naturally occurring biotic damage on leaf-level photosystem II operating efficiency (Φ_{PSII}) of 11 understory hardwood tree species using chlorophyll fluorescence and thermal imaging. Maps of fluorescence parameters and leaf temperature were stacked for each leaf and analyzed using a multivariate method adapted from the field of quantitative remote sensing. Two tree species, *Quercus velutina* and *Cercis canadensis*, grew in plots exposed to ambient and elevated atmospheric CO_2 and were infected with *Phyllosticta* fungus, providing a limited opportunity to examine the potential interaction of this element of global change and biotic damage on photosynthesis. Areas surrounding damage had depressed Φ_{PSII} and increased down-regulation of PSII, and there was no evidence of compensation in the remaining tissue. The depression of Φ_{PSII} caused by fungal infections and galls extended >2.5 times further from the visible damage and was ~40% more depressed than chewing damage. Areas of depressed Φ_{PSII} around fungal infections on oaks growing in elevated CO_2 were more than 5 times larger than those grown in ambient conditions, suggesting that this element of global change may influence the indirect effects of biotic damage on photosynthesis. For a single *Q. velutina* sapling, the area of reduced Φ_{PSII} was equal to the total area directly damaged by insects and fungi. Thus, estimates based only on the direct effect of biotic agents may greatly underestimate their actual impact on photosynthesis.

Keywords Biotic damage · Chlorophyll fluorescence imaging · Photosynthesis · Quantitative image analysis · Thermal imaging

Communicated by Robert Pearcy

M. Aldea
Program in Ecology and Evolutionary Biology, University of Illinois at Urbana-Champaign, Urbana, IL 61801, USA

J. G. Hamilton · J. P. Resti
Department of Biology, Ithaca College, Ithaca, NY 14850, USA

A. R. Zangerl · M. R. Berenbaum
Department of Entomology, University of Illinois at Urbana-Champaign, Urbana, IL 61801, USA

T. D. Frank
Department of Geography, University of Illinois at Urbana-Champaign, Urbana, IL 61801, USA

E. H. DeLucia (✉)
Department of Plant Biology, University of Illinois at Urbana-Champaign, 265 Morrill Hall (MC 116), 505 S. Goodwin Ave, Urbana, IL 61801, USA
e-mail: delucia@life.uiuc.edu

Introduction

Damage to photosynthetic tissue affects plant growth and the primary production of plant communities. Insect herbivory reduces net primary production in forests and grasslands by an average of 15 and 24%, respectively, and these values can exceed 70% during outbreaks (Cyr and Pace 1993). Calculating losses in production based on leaf area removed by herbivores may underestimate the actual reduction by as much as

2.6-fold (Lowman 1984). This underestimate comes primarily from the difference between the direct effect of herbivory (consumption of photosynthetic tissue) and the indirect effect—reduced photosynthesis in tissues not directly damaged by the herbivore (Welter 1989; Zangerl et al. 2002). In addition to herbivorous arthropods, pathogens (Hood et al. 1990; Osmond et al. 1990; Faeth 1992) and physical damage (Hoad et al. 1998; Hunter and Forkner 1999) can further reduce photosynthesis in natural ecosystems. For example, the reduction of stomatal conductance and photosynthesis by fungal infection of oak leaves directly reduces growth (Luque et al. 1999; El Omari et al. 2001).

Damage to foliage frequently initiates complex interactions between defense processes and photosynthesis. The induction of an arsenal of defense compounds (Karban and Myers 1989; Leon et al. 2001; Kessler and Baldwin 2002) can divert carbon and nitrogen away from primary metabolism (Agrawal et al. 2000), and many secondary compounds alter the photochemical status of the leaf. For example, changes in pigment content following mechanical damage (Herde et al. 1999) and the production of reactive oxygen species (Bi and Felton 1995; Thordal-Christensen et al. 1997; Leon et al. 2001; Bown et al. 2002) may reduce photosystem II quantum operating efficiency (Φ_{PSII}) and carbon assimilation rates in damaged leaves. Synthesis of defense compounds may take precedence over the maintenance of photosynthetic enzymes and growth, and damage may stimulate the expression of defense genes at the expense of those coding for rate-limiting constituents of photosynthetic metabolism (Schenk et al. 2000). Moreover, defenses against different classes of damage such as herbivores and pathogens may not offer cross-protection, thus exacerbating the costs of defense (Faeth 1992; Saikkonen et al. 2001). Indeed, the costs of defense may be great enough that leaf abscission becomes a viable alternative to defense (Hoad et al. 1998; Manter and Kavanagh 2003).

Elevated atmospheric CO_2, an important aspect of global change, can affect the interaction of plants with herbivores and pathogens. Increased availability of carbon can decrease the nitrogen content of tissues, thus decreasing their nutritional value to insects (Hunter 2001; Hamilton et al. 2004, 2005; Hall et al. 2005). The stimulation of photosynthesis by elevated CO_2 may also increase the allocation of carbohydrates to carbon-rich secondary metabolites, such as phenolics and terpenoids (Malmstrom and Field 1997; Ayres and Lombardero 2000; Hunter 2001; Karnosky et al. 2002). These changes in phytochemistry may not only alter trophic interactions between plants and their pathogens and herbivores (Malmstrom and Field 1997; Ayres and Lombardero 2000; Karnosky et al. 2002; Stiling et al. 2002; Hamilton et al. 2004, 2005; Knepp et al. 2005), but may also mediate the indirect responses of plants to damage (Ayres and Lombardero 2000). Although there is ample evidence that global atmospheric change may mediate both plant–pathogen and plant–insect interactions (Jiao et al. 1999; Jwa and Walling 2001; Karnosky et al. 2002; Hamilton et al. 2004, 2005; Knepp et al. 2005), the effects of localized biotic damage on the remaining tissue under elevated CO_2 are rarely addressed and the results are equivocal (Malmstrom and Field 1997; Jiao et al. 1999; Ayres and Lombardero 2000; Jwa and Walling 2001; Karnosky et al. 2002; Scherm 2004).

The objective of this research was to quantify the indirect effects of damage caused by biotic agents on photosynthesis, estimated by imaging chlorophyll fluorescence, in naturally occurring hardwood trees. This method permits non-invasive, spatially-resolved measurements of the component processes of photosynthesis across leaf surfaces (Oxborough 2004, 2005). The spatial pattern of temperature across leaf surfaces was also measured to determine if leaf damage affected the pattern of water loss. We hypothesized that different classes of damage (e.g., chewers, gall-forming arthropods, and fungal infections) would differentially affect chlorophyll fluorescence in the remaining leaf tissue. A novel application of multivariate analyses from remote sensing to fluorescence and thermal images of damaged leaves was used to test this hypothesis. Some plants grew in large plots exposed to elevated levels of atmospheric CO_2, providing a limited opportunity to examine how this element of global change may affect plant–insect and plant–pathogen interactions.

Materials and methods

Study site

The effect of biotic damage on photosynthesis was measured on naturally occurring saplings of hardwood trees (0.5–2 m height) growing in the understory of a 22-year-old loblolly pine (*Pinus taeda* L.) plantation at the Forest-Atmosphere Carbon Transfer and Storage 1 research site in the Piedmont region of North Carolina (35°58′N, 79°05′W). The plantation was dominated by loblolly pine (1,733 stems ha^{-1}; 92% of total woody biomass), with sweetgum (*Liquidambar styraciflua* L., 620 stems ha^{-1}) and tulip poplar (*Liriodendron tulipifera* L., 68 stems ha^{-1}) as sub-dominants (DeLucia et al. 1999). Forty-six other species of woody plants (trees,

shrubs, and vines) have established naturally in the understory of this forest (J. Pippen and W. Cook, unpublished data). This section of the Duke forest was farmed a century ago, and the current plantation was established in 1983 after a regenerating forest was clear-cut in 1979. The soil is a clay-rich Alfisol with low nitrogen and phosphorus availability (Schlesinger and Lichter 2001). According to data from the State Climate Office of North Carolina at North Carolina State University, mean monthly temperature and precipitation for the 2004 growing season (April–August) were 21.8°C and 100 mm (source station: KIGX, N.C., approximately 5 km SSE from the field site).

A free-air concentration enrichment system increases atmospheric CO_2 concentration in three 30-m-diameter experimental plots within this continuous pine forest (Hendrey et al. 1999). Fumigation with CO_2 in three "elevated" plots began in August 1996. Three "ambient" fully-instrumented control plots received the same volume of air without additional CO_2. Average CO_2 concentration in the understory (1 m height) was 386±27 μl l^{-1} (mean±1 SD) for ambient plots and 577±12 μl l^{-1} for elevated plots (Knepp et al. 2005).

Experimental design

Following an initial survey in early June 2004 of leaf damage on all woody plants in the experimental plots, five fully expanded leaves representing each damage type were selected on three to five saplings of each tree species. Because the density of damage was low and spatially heterogeneous, it was not always possible to choose leaves on different saplings and not all types of damage were found on all species in every experimental plot. Each damaged leaf was paired with a comparable undamaged leaf (on the same tree) to serve as a control. That damaged and "control" leaves were on the same plant opens the possibility that systemic responses may modulate fluorescence in the undamaged leaf. At least for *Quercus alba* and *Q. velutina*, the rate of CO_2 uptake and stomatal conductance in intact leaves were unaffected 1, 7, 30, and 60 days after manually damaging an adjacent leaf (50% area removal; data not shown). In total, we examined 15 damage types on 11 tree species growing in a forest understory (Table 1), some under ambient and elevated CO_2. Three classes of damage were represented: fungal infections, galls and chewing (all mandibulate feeders).

Chlorophyll fluorescence imaging

The spatial pattern of photosystem II operating efficiency (Φ_{PSII}) was quantified on attached leaves with an imaging chlorophyll fluorometer (Walz Imaging PAM, Walz GmbH, Effeltrich, Germany). The leaves were measured under steady state, light-adapted conditions (101 μmol m^{-2} s^{-1} PFD for black oak and 51 μmol m^{-2} s^{-1} PFD for all other species; 2.3×3.3 cm imaged area). These irradiances were typical for shaded understory conditions (average 121 μmol m^{-2} s^{-1}; median 68 μmol m^{-2} s^{-1}; Singsaas et al. 2000) and optimal for imaging chlorophyll fluorescence using the Walz Imaging PAM at its highest resolution. Each leaf was adapted to the new light environment for 5 min. The minimum fluorescence in the light-adapted state (F') was then recorded with the measuring pulse from the fluorometer (Baker et al. 2001). An image of the maximum fluorescence (F'_m) was recorded following a 1-s saturating pulse (ca. 2,500 μmol m^{-2} s^{-1}). Photosystem II efficiency (Φ_{PSII}) was calculated as the quotient $(F'_m - F')/F'_m$ (Baker et al. 2001; Oxborough 2004). At a given incident irradiance and leaf absorptance, Φ_{PSII} is directly proportional to the rate of electron transport through the photosystem II reaction centers and is correlated with the rate of carbon assimilation (Genty et al. 1989; Rolfe and Scholes 1995).

For species showing extensive suppression of photosynthesis near damaged areas (*Acer rubrum*, *Carya glabra*, *Cercis canadensis*, *L. tulipifera*, *Nyssa sylvatica*, and *Quercus velutina*), chlorophyll fluorescence quenching experiments were performed in a field laboratory using another imaging fluorometer (FluorImager, Technologica, Essex, UK) and an open-path gas-exchange system (Model 6400, LI-COR, Lincoln, Neb., USA). Leaves were cut in the field with their petioles under degassed water at ambient temperature (n=5 for each species of tree and damage type) and immediately transported to the laboratory, where they were placed in the gas-exchange cuvette under the imaging instrument as in Aldea et al. (2005). Following dark adaptation for 20–30 min, images of the minimum (F_o) and maximum (F_m) dark-adapted fluorescence yield were collected similarly to the light-adapted measurements. The maximum quantum efficiency of PSII in the dark-adapted state, F_v/F_m, was calculated as $(F_m - F_o)/F_m$ (Oxborough 2004). Because non-photochemical quenching is reversed during the dark treatment, the value of F_v/F_m is influenced only by the photochemical status of PSII reaction centers. Decreases in this parameter are proportional to decreases in the rate constant for photochemistry and indicate direct damage to photosystem II reaction centers (Oxborough 2004). Leaves were then exposed to actinic light (101 μmol m^{-2} s^{-1} PFD; 10×12 cm imaged area) for 30 min, and images of F' and F'_m were acquired as described above. In addition to Φ_{PSII}, down-regulation

Table 1 The effect of different biotic agents, including fungal infection, insect galls and chewing damage by insects, on the quantum efficiency of electron transport through Photosystem II (Φ_{PSII}) on leaf tissue adjacent to the site of direct damage

Tree species	Damage type (*n*)	Area		Propagation (mm)	Φ_{PSII}		
		Visible injury (cm^2)	Halo/damage		Control	Damaged	Halo
Chewing damage							
Carya glabra[a]	Unknown leaf tier (2)	6.7±0.2 [b]	0	0	0.73±0.00	0.71±0.02[c]	0.70±0.02[d]
C. tomentosa	Unknown skeletonizer (5)	0.98±0.13	1.56±0.47	2.6±1.8	0.65±0.00	0.66±0.00	**0.62±0.01**
Liriodendron tulipifera[a]	Unknown leaf miner (2)	1.30±0.25	0	0	0.69±0.01	0.70±0.00	N/A
Quercus alba	Unknown skeletonizer (6)	2.32±1.07	0.12±0.05	0.5±0.06	0.64±0.00	0.64±0.00	**0.60±0.01**
Ulmus alata	Elm leaf beetle (skeletonizer) (5)	1.14±0.40	0.35±0.20	0.7±0.2	0.54±0.01	0.55±0.01	**0.44±0.02**
U. alata[a]	Agromyzidae leaf miner (5)	0.58±0.10	0	0	0.59±0.01	0.60±0.00	N/A
Fungal infections							
Acer rubrum	*Phyllosticta* fungus (5)	0.29±0.13	0.73±0.42	1.5±0.6	0.65±0.00	0.65±0.00	**0.62±0.00**
Cercis canadensis	*Cercospora* fungal spot (5)	0.49±0.07	0.77±0.19	1.8±0.3	0.52±0.01	0.54±0.01	**0.42±0.02**
C. canadensis[a]	*Cercospora* fungal spot (5)	0.62±0.08	0.69±0.08	1.5±0.1	0.57±0.02	0.60±0.01	0.54±0.01
Malus sp.[a]	Cedar apple rust (*Gymnosporangium*) (5)	0.59±0.09	0.24±0.08	0.7±0.1	0.61±0.01	0.62±0.00	**0.47±0.04**
Liquidambar styraciflua[a]	*Cercospora* fungal spot (5)	0.04±0.02	27.5±8.3	2.5±0.5	0.66±0.01	0.66±0.01	**0.60±0.02**
L. tulipifera[a]	Unknown fungal spot (5)	0.36±0.04	1.36±0.32	3.0±0.6	0.61±0.01	0.62±0.00	**0.57±0.01**
Q. alba[a]	Unknown fungal spot (5)	0.30±0.05	0.31±0.10	0.7±0.2	0.61±0.01	0.58±0.00	**0.52±0.01**
Q. velutina	*Phyllosticta* fungus (5)	0.17±0.04	0.53±0.21	0.1±0.02	0.44±0.01	0.46±0.00	**0.37±0.02**
Q. velutina[a]	*Phyllosticta* fungus (6)	0.57±0.21	5.82±0.78	8.1±1.7	0.45±0.01	0.46±0.01	**0.39±0.01**
Galls							
A. rubrum	Aborted mite gall (4)	0.72±0.09	0.72±0.36	1.9±0.5	0.56±0.01	0.55±0.02	**0.47±0.00**
C. glabra	"*Cecidomyia*" glutinosa midge—old (9)	0.21±0.07	0.15±0.06	0.5±0.12	0.64±0.01	0.66±0.01	**0.59±0.01**
C. glabra	*Caryomyia* midge abaxial galls (7)	0.05±0.01	50.9±11.8	13.7±1.2	0.60±0.02	0.61±0.02	**0.54±0.02**
C. glabra	"*Cecidomyia*" glutinosa midge— recent (5)	0.47±0.07	0.20±0.03	0.5±0.11	0.56±0.00	0.54±0.02	**0.36±0.04**
C. tomentosa	*Caryomyia* midge adaxial galls (5)	0.02±0.01	0	0	0.64±0.00	0.65±0.00	N/A
Nyssa sylvatica[a]	*Eriophyes nyssae* mite galls (5)	0.66±0.20	0	0	0.61±0.00	0.65±0.01	N/A
Q. velutina	Cynipid wasp gall (5)	0.02±0.01	11.2±1.7	1.5±0.03	0.44±0.01	0.46±0.00	**0.35±0.02**
Q. velutina[a]	Cynipid wasp gall (4)	0.04±0.01	11.1±2.0	3.8±0.9	0.45±0.01	0.47±0.00	**0.38±0.00**
U. alata	Eriophyidae mite galls (5)	0.79±0.56	0.77±0.58	0.7±0.5	0.58±0.03	0.61±0.02	**0.52±0.02**

"Visible damage" represents the area (cm^2) of direct damage and the "Halo/damage" ratio represents the total area of depressed Φ_{PSII} divided by the area of direct damage (visible damage). "Propagation" is the average linear distance (mm) from the edge of visible damage where Φ_{PSII} was depressed. "Control", "Damaged" and "Halo" represent the average Φ_{PSII} of undamaged leaves, the average Φ_{PSII} of undamaged portions of damaged leaves, and the average Φ_{PSII} within the halo of suppressed photosynthesis around direct, visible damage, respectively. Values represent least square means (*n* specified in parentheses for each damage type and species)±1 SE

Bold-face values were significantly different from control at the $P<0.05$ level

N/A Not applicable

[a] These measurements were performed on plants growing under elevated CO_2 at 577 μmol mol^{-1} (see Materials and methods)

[b] Area of overlap between the two tied leaves

[c] Top leaf

[d] Bottom leaf

of PSII was quantified as Stern-Volmer non-photochemical quenching of fluorescence (NPQ) calculated as F_m/F'_m-1 (Oxborough 2004). This parameter is proportional to the amount of non-photochemical energy dissipation by PSII reaction centers either as non-radiative decay or heat through the xanthophyll cycle (Horton et al. 1996). Measurements were completed within 1 h of harvesting leaves from the field. In this time, stomatal conductance, carbon assimilation rates and values for chlorophyll fluorescence of cut leaves measured in the laboratory were comparable to values measured on attached leaves in the field

under similar environmental conditions (data not shown).

Thermal imaging

To quantify the spatial pattern of evapotranspiration we collected images of leaf surface temperature with an infrared camera (ThermaCAM SC1000 Infrared Camera, FLIR Systems, Portland, Ore., USA; wavelengths 3–5 μm). We assumed that the variation in latent heat loss associated with evapotranspiration was the dominant process controlling variation in leaf surface temperature (Jones 1999; Omasa and Takayama 2003). The adaxial surface of an attached, shaded leaf was held perpendicular to the camera and in front of a warmer background to improve contrast (ca. 30°C; 15–20 cm behind the leaf). The thermal camera was calibrated for air temperature and humidity and leaf emissivity was assumed to be 1. Temperature differences on the same image were precise to ±0.07°C (instrument specifications). Thermal images were analyzed by subtracting the temperature of areas close to damage (coincident with the Φ_{PSII} halos) from areas away from damage for each image separately, thus eliminating the need for direct comparison between different thermal images.

Feeding trials

To investigate whether the indirect effects of herbivory on chlorophyll fluorescence depended on the time since damage, we performed feeding trials on two tree species. We placed a polyphemus caterpillar (*Antheraea polyphemus* Cramer) in a mesh bag on each of five leaves of *Q. velutina* on five separate trees. Similarly, we placed redhumped caterpillars (*Schizura concinna* J.E. Smith) on leaves of *C. canadensis* (n=5). Both insect species are generalist herbivores that consume the leaf lamella while avoiding large veins. The insects were removed the following day after they had eaten 10–60% of the leaf area. The spatial patterns of chlorophyll fluorescence and leaf surface temperature were quantified as described above.

Image analysis

The spatial patterns of chlorophyll fluorescence and leaf surface temperature were quantified using an image analysis software package (Erdas Imagine 8.6, Leica Geosystems GIS & Mapping LLC, Atlanta, Ga., USA). We applied well-established and widely-used analytical methods from the field of remote sensing, as described by Swain and Davis (1978), to images representing physiological processes. The extent of visible damage and halos of suppressed Φ_{PSII} around areas of visible damage, as well as the spatial average of Φ_{PSII} and temperature were quantified after an iterative neighborhood procedure automatically identified contiguous pixels with similar properties around a manually-defined starting point (Region Grow Tool, Erdas Imagine 8.6). This procedure used pixel intensity values in an image to form clusters of similar, contiguous pixels. Pixel intensity values in an image were linearly related to their Φ_{PSII} or temperature values (i.e., R^2>0.99). An area of the leaf around damage was considered depressed if its operating efficiency was lower than the average Φ_{PSII} of its respective control leaf. The propagation of damage near each fungal spot, gall and hole was quantified individually as the average of five random measurements of the radial distance between the edge of visible damage and the perimeter of the zones where Φ_{PSII} was suppressed.

For the quenching analysis, images of Φ_{PSII}, NPQ, and leaf surface temperature were overlaid in a virtual stack, following a first-degree polynomial transformation that ensured accurate spatial overlap among the layers in the image. These images were analyzed using an iterative self-organizing multivariate clustering algorithm (ISODATA, Erdas Imagine 8.6; Swain and Davis 1978), which created clusters of pixels with similar intensities based on data from the three overlapped images (Fig. 3). Within each cluster returned by the ISODATA procedure, it was possible to examine the covariance of the data from the overlaid images, thus allowing a statistical analysis of spatial patterns of various processes mapped with different techniques and instruments. Clusters represented spatial features on the leaf surface based on their photosynthetic efficiency, NPQ and temperature. A map of the spatial pattern of the clusters was made by assigning each pixel in the image to a cluster using Bayes maximum likelihood decision rules (Swain and Davis 1978).

Statistical analysis

Differences in the thermal, chlorophyll fluorescence, and damage propagation data among damage classes were evaluated by an analysis of variance (Proc Mixed, SAS 9.1, SAS Institute, Cary, N.C., USA). Because damage was highly heterogeneous among individual trees, we assumed individual leaves provided independent measurements (n=5–10). Damage class (fungal, galls, or chewing) and measurement type (control or damaged) were the independent variables, while temperature, Φ_{PSII} and area of depressed photosynthetic efficiency were dependent variables. Because damage

classes were unevenly distributed among tree species, a full-factorial analysis of variance on the entire data set was not possible. To determine whether there were compensatory increases in Φ_{PSII} in the undamaged portions of damaged leaves, analyses of variance were performed for every tree species individually. Potential differences among species in Φ_{PSII} and the spatial extent of damage were examined within each damage class separately. Another ANOVA was run to detect a possible interaction of elevated CO_2 and biotic damage for *C. canadensis* and *Q. velutina*. These were the only two tree species with the same damage type on saplings growing in both ambient and elevated CO_2 plots. Statistical significance was recognized at $P \leq 0.05$. When the overall P was significant, post hoc multiple comparisons were conducted with the Tukey-Kramer test.

Results

Damage caused by biotic agents was observed on foliage of 11 of the 46 species of hardwood trees growing in the forest understory and was broadly categorized into three classes: (1) damage caused by fungi; (2) galls caused by wasps (Hymenoptera), midges (Diptera) and mites (Acari); and (3) chewing and skeletonizer damage, including leaf tiers (Table 1). Although identification of the biotic agents causing leaf damage to the level of species was not always possible and may have varied within a damage type, chewing insects that were most abundant in the experimental plots were from the orders Coleoptera, Lepidoptera, and Orthoptera (Hamilton et al. 2004). "Leaf tier" damage was evident only on *C. glabra*. Where possible, damage was further categorized visually as "recent" or "old" (D. Stephan and T. Creswell, personal communication).

Depending on the type of damage and tree species, biotic damage caused a decrease in the operating efficiency of photosystem II (Φ_{PSII}) at considerable distance away from the zone of visible damage (Fig. 1, Table 1). The Φ_{PSII} of the undamaged portions of damaged leaves was not significantly different from control leaves ($P>0.05$), so we did not observe compensatory increases in photosynthesis in response to damage. Fungal infections on *C. canadensis* and galls on *C. glabra* reduced Φ_{PSII} by 22 and 33%, respectively, and the damage extended up to 14 mm away from the tissue affected visibly (Figs. 1, 2). *Phyllosticta* fungal infections on *Q. velutina* growing in plots exposed to elevated CO_2 were surrounded by large areas of depressed photosynthetic efficiency (i.e., halos), while the visible damage and the region of depressed Φ_{PSII} for similarly infected *A. rubrum* were smaller and more localized (Table 1). In many cases, small galls caused significant depressions of Φ_{PSII} over extensive areas of surrounding leaf tissue (Fig. 1c,d), and these areas of depressed photosynthetic efficiency were generally associated with lower leaf surface temperature (Fig. 2) and higher non-photochemical energy dissipation from PSII (i.e., NPQ; Fig. 3d). With the exception of *A. rubrum*, fungal spots also showed extensive depression of Φ_{PSII}, but these areas exhibited increased NPQ and leaf temperature (Figs. 1, 2, 3b,d,f), relative to leaf tissue at considerable distance from the areas of direct damage. Skeletonized damage to *Q. alba* leaves (Fig. 1e, f) and chewing damage (leaf miners) to *L. tulipifera* leaves caused localized or no inhibition of Φ_{PSII}, while fungal spots on these species were surrounded by large halos of suppressed Φ_{PSII} (Table 1).

In the feeding trial, the reduction of Φ_{PSII} following the removal of *A. polyphemus* and *S. concinna* larvae from leaves of *Q. velutina* and *C. canadensis*, respectively, was localized near the tissue that was removed, and was similar to older, naturally occurring damage by chewing insects (data not shown).

The zone of reduced Φ_{PSII} caused by fungal infections and galls extended further from the visible damage ($P=0.04$) and Φ_{PSII} was lower ($P<0.01$) than near

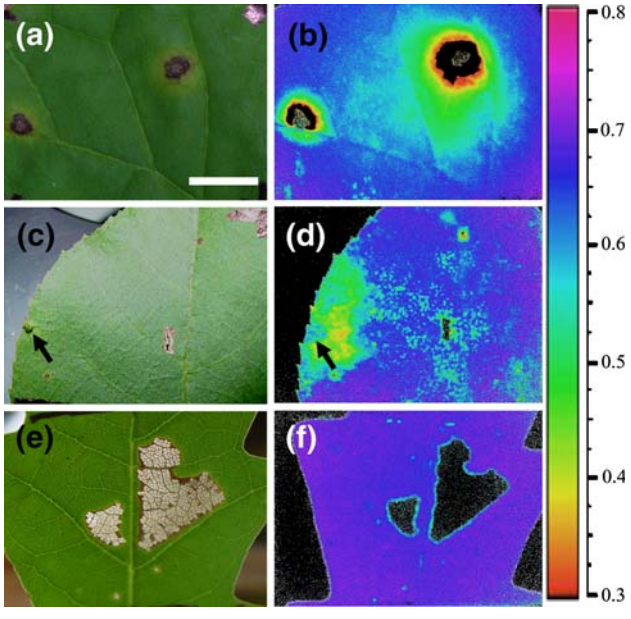

Fig. 1 Representative true-color reflected light images (*left column*) and false color images (*right column*) of the spatial patterns of Φ_{PSII} for fungal infection of a *Cercis canadensis* leaf (**a**, **b**), damage caused by *Caryomyia* midge galls on a *Carya glabra* leaf (**c**, **d**), and skeletonizer damage to a *Quercus alba* leaf (**e**, **f**). The *color scale* represents values of Φ_{PSII} (fractional values). All images are on the same scale and the *bar* in image (**a**) represents 1 cm

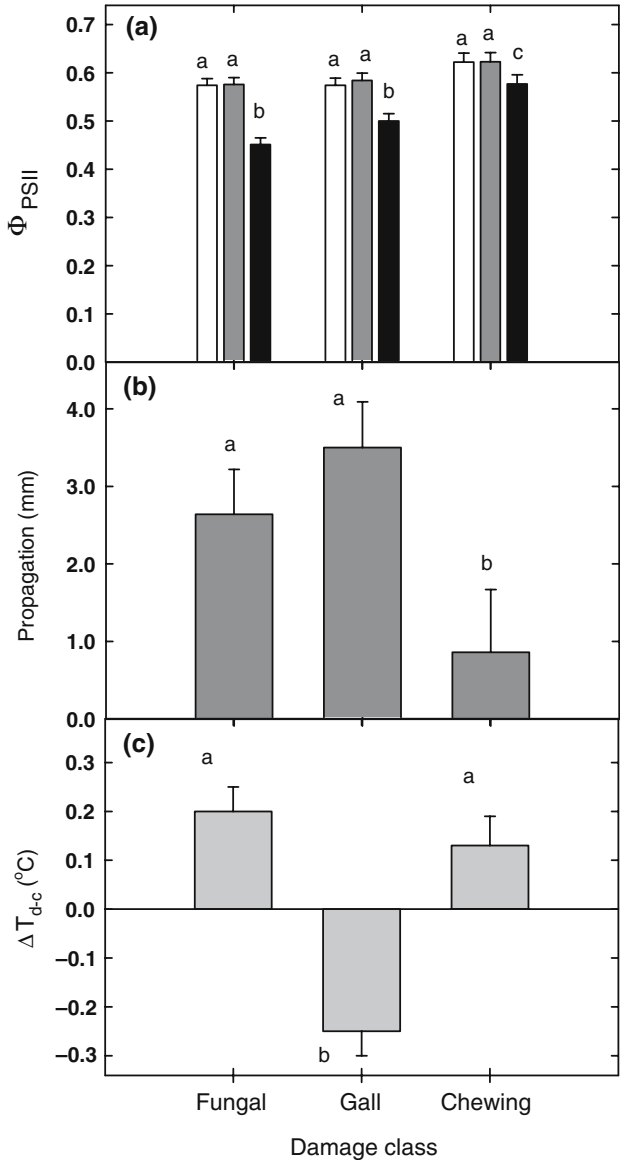

Fig. 2 The indirect effects of three classes of biotic damage (fungal, gall, chewing) on leaves of understory hardwood trees. **a** Photosystem II operating efficiency (Φ_{PSII}). The *open bars* represent values of Φ_{PSII} for undamaged leaves, the *gray bars* represent values of Φ_{PSII} for unaffected portions of damaged leaves, and the *black bars* represent values of Φ_{PSII} in the regions surrounding visible damage where photosynthesis was suppressed. **b** Propagation was the distance that depressed photosynthesis extended away from the site of visible damage. **c** The difference in leaf surface temperature of areas close to the site of direct damage and of areas away from direct damage where Φ_{PSII} had returned to control values. *Bars* represent least squared mean values (n=25–49) for each damage class (±1 SE), and *bars with different letters* were statistically different at the $P \leq 0.05$ level

chewing damage (Fig. 2). Of all classes of damage, galls had the largest halos of depressed Φ_{PSII} when normalized to the size of visible injury (P=0.03), while chewing rarely affected the Φ_{PSII} of surrounding tissue and only over small distances (Table 1, Figs. 1, 2). The surface temperatures of leaf regions where Φ_{PSII} was depressed around fungal and chewing damage were higher than remaining leaf tissue, while the areas around galls were cooler (Fig. 2c).

To estimate the relative areas of leaf tissue damaged directly by biotic agents versus the area with reduced values of Φ_{PSII} for a naturally occurring understory tree, we photographed all leaves (ca. 200) on a *Q. velutina* sapling (3 m height) with a digital camera. Damaged leaf area and total leaf area were quantified with the image analysis procedure described by Hamilton et al. (2004). The total area of depressed Φ_{PSII} was calculated by applying the Halo/Damaged area ratios in Table 1 to each damage type separately and summing the damaged area. Visible damage (all damage types) occurred on 6.8% of the total leaf area and the total area of depressed Φ_{PSII} was 6.8% of the remaining leaf area.

The responses of different tree species to the three different classes of damage were analyzed statistically only for those species growing in the ambient [CO_2] plots, as there were insufficient data to extend this analysis to saplings growing in the elevated [CO_2] plots. We were unable to resolve statistical differences in the propagation of damage or the area of depressed Φ_{PSII} (halo/damage area ratio) around fungal and gall infections among the tree species. For chewing damage, however, *Carya tomentosa* had a significantly larger halo/damage area ratio than *Q. alba* and *U. alata* (P=0.01; Table 1). The magnitude of depression of Φ_{PSII} around visible damage varied among tree species for all damage classes. For chewing damage, Φ_{PSII} surrounding visible damage was significantly more depressed for *U. alata* than for *C. tomentosa* and *Q. alba* (P<0.01), though it was depressed over a smaller area. Among species with fungal infections, the area surrounding visible damage on leaves of *A. rubrum* operated at a significantly higher Φ_{PSII} than *C. canadensis* and *Q. velutina* (P<0.01), while the area over which photosynthesis was depressed was comparable among the three species. For gall damage, *Q. velutina* had the greatest depression of Φ_{PSII} (P<0.01).

By overlapping images of Φ_{PSII}, NPQ, F_v/F_m, and leaf surface temperature, it became evident that the depression of photosynthetic efficiency surrounding galls and fungal spots for *A. rubrum*, *C. glabra*, *C. canadensis*, *L. tulipifera*, *N. sylvatica,* and *Q. velutina* was only partially related to physical damage to PSII reaction centers (F_v/F_m) but was closely associated with increased non-photochemical energy dissipation (Fig. 3g). Depressions of F_v/F_m were only observable in

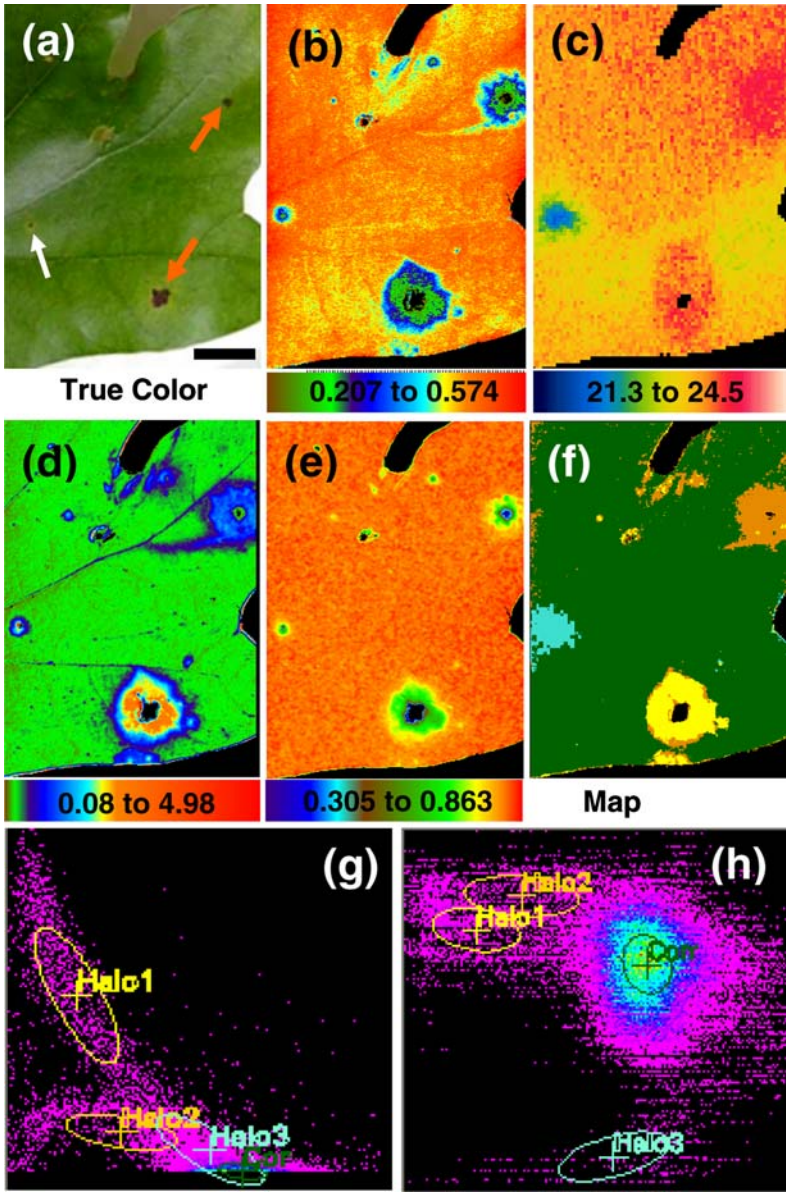

Fig. 3 The spatial pattern of chlorophyll fluorescence parameters and leaf temperature, and a map image derived from quantitative image analysis for a *Quercus velutina* leaf with two *Phyllosticta* fungal spots (*orange arrows*) and a cynipid wasp gall (*leftmost spot*, *white arrow*). **a** Reflected light image; **b** false color image of Φ_{PSII} (scale below); **c** false color thermal image of the same leaf (scale below in °C) after registration to the same coordinate system as the fluorescence images (see Materials and methods). The three images, Φ_{PSII}, NPQ and thermal, were "stacked" and subjected to a multivariate clustering algorithm to create the map image (**f**). **d** False color image (scale below) of the Stern-Volmer quenching parameter, NPQ; **e** false color image of the dark-adapted F_v/F_m fluorescence parameter; **f** An image map derived from a multivariate clustering algorithm (ISODATA) that classified all pixels of the image into four classes based on their intensity in the overlaid Φ_{PSII}, NPQ and thermal images. Green regions of the map represents areas that were operating at control values for all parameters (denoted *Control*), *yellow areas* were pixels with similar properties as those in the immediate vicinity of the old fungal spot (denoted *Halo1*), *orange areas* were pixels similar to those close to the more recent fungal spot at the top of the image (*Halo2*), while *light-blue* pixels were those close to the cynipid wasp gall (*Halo3*); **g** a feature-space diagram plotting the intensities of all pixels in the image stack used for analysis: Φ_{PSII} is plotted on the *x*-axis and NPQ on the *y*-axis. Ellipses for each cluster (1−SD) were overlaid on this plot to evaluate the spectral properties of each class. All *Halo* classes displayed decreased Φ_{PSII} and increased NPQ compared to the *Control* class; **h** a feature-space diagram of Φ_{PSII} (*x*-axis) versus thermal (*y*-axis), as described above. *Halo1* and *Halo2* have similar properties with respect to these two factors, but *Halo3* is much cooler than the control area in the center of the plot. Thermal data did not significantly correlate with Φ_{PSII} for *Halo1* and *Halo2*, but were slightly related for *Halo3* (R=0.6, P<0.01). The color scale of feature-space plots represents the density of pixels plotted in a particular location; the gradient from no pixels to most pixels is illustrated by the color continuum: *black*, *purple*, *blue*, *cyan*, *yellow* and *orange*. The clusters plotted in (**g**) and (**h**) with respect to their spectral properties were mapped spatially in (**f**). All images are on the same scale and the *bar* in (**a**) represents 1 cm

the immediate vicinity of visible damage, over areas generally much smaller than the region where Φ_{PSII} was depressed (Fig. 3e). In contrast, substantial areas of down-regulation of PSII (NPQ) had complete spatial overlap and a significant correlation with areas of depressed Φ_{PSII} around fungal spots (*C. canadensis, L. tulipifera*, and *Q. velutina*; n=5–6 for each tree species) and galls (*A. rubrum*, *C. glabra*, *N. sylvatica,* and *Q. velutina*; n=4–9 for each tree species). Although the depression of Φ_{PSII} around fungal infections and galls both overlapped increases in NPQ (Fig. 3g), leaf surface temperature was higher in the vicinity of fungal spots but lower around galls (Fig. 3h). These differences were graphically illustrated by the map image (Fig. 3f), which spatially renders the location of the clusters returned by the Bayes maximum likelihood classification. The map image shows that the areas of depressed photosynthetic efficiency around recent and old fungal spots had some statistical overlap, but there were no shared characteristics between the area around fungal infections and the area surrounding galls (Fig. 3f).

The effect of CO_2 on the propagation of damage was inconsistent and depended on the plant species and type of damage. For *Q. velutina* infected with *Phyllosticta* fungus, the areas of depressed Φ_{PSII} on leaves from plants grown in elevated CO_2 were more than five times larger than leaves grown in ambient conditions (P<0.01), but there was no effect on the values of Φ_{PSII} within the halos (P=0.56). In contrast, there was no effect of growth under elevated CO_2 on the depth of the depression of Φ_{PSII} or the propagation of damage for leaves of *Q. velutina* with wasp galls or leaves of *C. canadensis* with fungal infection (P>0.05; Table 1).

Discussion

Chewing damage and fungal and gall infections differentially affected the component processes of photosynthesis of nearby leaf tissue (Table 1). Fungal infections and galls caused large depressions (>25%) of photosynthetic efficiency (Φ_{PSII}) over extended areas of the leaf around the visible damage (Figs. 1, 2). The quantitative analysis of spatial maps of fluorescence quenching parameters indicated that the depression of Φ_{PSII} in the vicinity of fungal spots and galls was partially caused by physical damage to PSII reaction centers and had a complete spatial coincidence with areas of increased down-regulation of Photosystem II (NPQ). In contrast, chewing damage resulted in minor (~7%) depressions of Φ_{PSII} that were restricted to 1 mm from the edge of holes (Figs. 1, 2). Depending on the type of damage and tree species involved, an evaluation based solely on visible injury or missing tissue may greatly underestimate the ecological impact of biotic agents on photosynthesis in the understory trees.

Investigation of factors generating spatial variation in photosynthesis typically employs analysis of single two-dimensional images (e.g., Omasa and Takayama 2003; Smith et al. 2004). While effectively quantifying the pattern of variation, this approach provides limited information about the factors generating spatial heterogeneity. Image analysis tools developed for remote sensing permitted for the first time the assembly of multiple images each representing a different physiological process, thus affording novel insight into the mechanisms governing the effect of biotic damage on photosynthesis. Precisely aligning and overlapping images (e.g., thermal and chlorophyll fluorescence) permitted a pixel-for-pixel analysis of covariance between different physiological processes (Fig. 3) and revealed that galls and fungi affected photosynthesis by different mechanisms. An increase in NPQ (Fig. 3d) contributed to extensive regions of reduced Φ_{PSII} around areas of fungal damage and wasp galls (Fig. 3b). However, the surrounding tissue was warmer near fungal infections but cooler near galls (Fig. 3c). Although data from this field survey do not permit a thorough exploration of the mechanisms underlying the propagation of reduced Φ_{PSII} across leaf surfaces, image analysis methods can accommodate additional layers (images) representing other physiological processes, thus strengthening inferences about mechanisms.

Although similar in their effect on electron transport through PSII, the indirect effects of fungal and gall infections on photosynthesis operate through different mechanisms. A reduction in stomatal conductance and associated decline in intercellular CO_2 concentration may have contributed to the depression of Φ_{PSII} surrounding fungal spots. Insofar as leaf surface temperature is proportional to evapotranspiration rates, the higher temperature of areas around fungal spots (Figs. 2, 3) suggests that the infection caused a reduction in stomatal conductance. Stomatal closure contributes to depressed PSII efficiency and increased NPQ under physiological conditions, as well as chemical and pathogen stress (Daley et al. 1989; Dai et al. 1992; Daley 1995; Guidi et al. 1997; Osmond et al. 1998). Pathogen-derived toxins (Schulz et al. 2002; De Boer 2003), a hypersensitive response that includes localized production of H_2O_2, superoxide radicals, and other reactive oxygen species (Bi and Felton 1995; Thordal-Christensen et al. 1997; Repka 2002; Fryer et al. 2003),

or defense-related down-regulation of photosynthesis (Bi and Felton 1995; Schenk et al. 2000; Bostock et al. 2001) may also have contributed to the down-regulation and physical damage to PSII surrounding fungal spots. Peterson and Aylor (1995) concluded that following pathogen infection, the eventual chlorosis or necrosis of infected areas was caused by the failure of photoprotective mechanisms leading to physical damage to the photosynthetic machinery.

Galls also were surrounded by large areas of depressed Φ_{PSII}, increased NPQ, and physical damage to PSII reaction centers (Fig. 3). Unlike fungal infection, the depression of Φ_{PSII} near galls was probably not related to stomatal closure, as the temperature of the surrounding tissue was lower than the rest of the leaf, indicative of higher transpiration rates (Figs. 2, 3). Altered water transport around fusiform rust galls on loblolly pine may increase nutrient transport to the developing pathogen (Macfall et al. 1994).

Chewing damage caused only mild and localized suppressions of the photosynthetic efficiency of adjacent tissue (Table 1, Fig. 2). The higher temperature of these areas (Fig. 2) was most likely caused by the desiccation of tissue along the edges of damage, as previously reported for insect herbivory in soybean (Aldea et al. 2005). In contrast to the trees examined in this study, chewing damage in wild parsnip (*Pastinaca sativa* L.) caused dramatic reduction of Φ_{PSII} extending considerable distances from cut edges (Zangerl et al. 2002). The suppression of Φ_{PSII} in regions of the leaf near the tissue removed by caterpillars was related to increases in the production of defense compounds (Zangerl et al. 2002), some of which are strongly autotoxic and directly inhibit Φ_{PSII} (Gog et al. 2005). Chewing damage by cabbage looper (*Trichoplusia ni*; Lepidoptera: Noctuidae) larvae also caused substantial reductions in Φ_{PSII} at some distance from the tissue removed (Tang et al. 2006). In this case, it appeared that nearby tissues became isolated from the water supply and became desiccated.

Although we were unable to resolve consistent differences within a damage class, the indirect effects of biotic damage appeared variable among tree species. For example, the photosystem II efficiency (Φ_{PSII}) in areas around chewing damage was more depressed for *U. alata* ($P<0.01$) growing under ambient atmospheric CO_2 than other species subjected to chewing damage under the same atmospheric conditions (Table 1), while Φ_{PSII} near galls was less depressed on *A. rubrum* leaves compared to other species suffering similar damage. The region of depressed Φ_{PSII} extended considerably further from chewing damage to *C. tomentosa* leaves than for other species with similar damage. A firm conclusion that the photosynthetic response to damage varied systematically among tree species is not supported by our results and would require controlled comparisons of the response to the same type of damage.

By altering the chemical and physiological properties of leaves, exposure to elevated CO_2 may modulate the propagation of damage from biotic agents. Only two tree species, *Q. velutina* and *C. canadensis*, experienced the same type of damage in plots exposed to ambient and elevated CO_2. At least for *Q. velutina* infected with *Phyllosticta* fungus, the area of depressed Φ_{PSII} in elevated CO_2 plots was ~ 5 times larger than on trees growing in ambient plots (Table 1). Enhanced synthesis of tannins and phenolic compounds in response to damage and elevated CO_2 (Lindroth et al. 1993; Shure et al. 1998; Hunter and Forkner 1999; Cornelissen et al. 2003; Knepp et al. 2005) may interfere with the repair of damaged photosynthetic reaction centers, thus amplifying the indirect effects of fungal infections on photosynthetic electron transport. However, elevated CO_2 had no effect on the propagation of damage caused by cynipid wasp galls on *Q. velutina* or *Cercospora* fungal infection of *C. canadensis*. These limited observations do not permit an unambiguous understanding of the potential effects of CO_2 on the photosynthetic response to biotic agents.

In so far as it is related to the rate of net photosynthesis, depressed Φ_{PSII} caused by fungal or gall infections in areas adjacent to the injuries may reduce carbon acquisition and productivity. For one sapling where biotic damage on every leaf was quantified, the area of suppressed Φ_{PSII} (indirect damage) was equal to the total area directly affected by insects and fungi, suggesting that models relying solely on visible damage may substantially underestimate the effects of biotic damage. With the rapid development of new imaging techniques in plant physiology, quantitative image analysis provides an invaluable tool for revealing the mechanisms contributing to the indirect effects of biotic damage on photosynthesis.

Acknowledgements We thank H. Bohnert of the University of Illinois at Urbana-Champaign (UIUC) for the use of the thermal camera, and D. Stephan and T. Creswell (North Carolina State University–Plant Disease and Insect Clinic) for identifying insect and fungal damage. We also thank D. Moore, M. Prater, R. Knepp, O. Dermody, N. Morphew and J. Tang (UIUC) for their insightful comments on an earlier version of this manuscript, and L. Monroe (Ithaca College) and R. Bhayana (UIUC) for assistance with image analysis. This research was supported by a grant from the National Science Foundation (IBN 0236053). The experiments described herein were in compliance with all applicable US federal, NC state, and local laws at the time when they were performed.

References

Agrawal AA, Karban R, Colfer RG (2000) How leaf domatia and induced plant resistance affect herbivores, natural enemies and plant performance. Oikos 89:70–80

Aldea M, Hamilton JG, Resti JP, Zangerl AR, Berenbaum MR, DeLucia EH (2005) Indirect effects of insect herbivory on leaf gas exchange in soybean. Plant Cell Environ 28:402–411

Ayres MP, Lombardero MJ (2000) Assessing the consequences of global change for forest disturbance from herbivores and pathogens. Sci Total Environ 262:263–286

Baker NR, Oxborough K, Lawson T, Morison JIL (2001) High resolution imaging of photosynthetic activities of tissues, cells and chloroplasts in leaves. J Exp Bot 52:615–621

Bi JL, Felton GW (1995) Foliar oxidative stress and insect herbivory: primary compounds, secondary metabolites, and reactive oxygen species as components of induced resistance. J Chem Ecol 21:1511–1529

Bostock RM, Karban R, Thaler JS, Weyman PD, Gilchrist D (2001) Signal interactions in induced resistance to pathogens and insect herbivores. Eur J Plant Pathol 107:103–111

Bown AW, Hall DE, MacGregor KB (2002) Insect footsteps on leaves stimulate the accumulation of 4-aminobutyrate and can be visualized through increased chlorophyll fluorescence and superoxide production. Plant Physiol 129:1430–1434

Cornelissen T, Stiling P, Drake B (2003) Elevated CO_2 decreases leaf fluctuating asymmetry and herbivory by leaf miners on two oak species. Global Change Biol 10:27–36

Cyr H, Pace ML (1993) Magnitude and patterns of herbivory in aquatic and terrestrial ecosystems. Nature 361:148–150

Dai ZY, Edwards GE, Ku MSB (1992) Control of photosynthesis and stomatal conductance in *Ricinus communis* L (castor bean) by leaf to air vapor-pressure deficit. Plant Physiol 99:1426–1434

Daley PF (1995) Chlorophyll fluorescence analysis and imaging in plant stress and disease. Can J Plant Pathol 17:167–173

Daley PF, Raschke K, Ball JT, Berry JA (1989) Topography of photosynthetic activity of leaves obtained from video images of chlorophyll fluorescence. Plant Physiol 90:1233–1238

De Boer SH (2003) Characterization of pectolytic erwinias as highly sophisticated pathogens of plants. Eur J Plant Pathol 109:893–899

DeLucia EH et al (1999) Net primary production of a forest ecosystem with experimental CO_2 enrichment. Science 284:1177–1179

El Omari B, Fleck I, Aranda X, Moret A, Nadal M (2001) Effect of fungal infection on leaf gas-exchange and chlorophyll fluorescence in *Quercus ilex*. Ann For Sci 58:165–174

Faeth SH (1992) Interspecific and intraspecific interactions via plant-responses to folivory—an experimental field test. Ecology 73:1802–1813

Fryer MJ, Ball L, Oxborough K, Karpinski S, Mullineaux PM, Baker NR (2003) Control of *Ascorbate Peroxidase 2* expression by hydrogen peroxide and leaf water status during excess light stress reveals a functional organisation of *Arabidopsis* leaves. Plant J 33:691–705

Genty B, Briantais JM, Baker NR (1989) The relationship between the quantum yield of photosynthetic electron-transport and quenching of chlorophyll fluorescence. Biochim Biophys Acta 990:87–92

Gog L, Berenbaum MR, DeLucia EH, Zangerl AR (2005) Autotoxic effects of essential oils on photosynthesis in parsley, parsnip and rough lemon. Chemoecol 15:115–119

Guidi L, Nali C, Ciompi S, Lorenzini G, Franco G (1997) The use of chlorophyll fluorescence and leaf gas exchange as methods for studying the different responses to ozone of two bean cultivars. J Exp Bot 48:173–179

Hall MC, Stiling P, Moon DC, Drake BG, Hunter MD (2005) Effects of elevated CO_2 on foliar quality and herbivore damage in a scrub oak ecosystem. J Chem Ecol 31:267–286

Hamilton JG, Zangerl AR, Berenbaum MR, Pippen JP, Aldea M, DeLucia EH (2004) Insect herbivory in an intact forest understory under experimental CO_2 enrichment. Oecologia 138:566–573

Hamilton JG, Dermody O, Aldea M, Zangerl AR, Rogers A, Berenbaum MR, DeLucia EH (2005) Anthropogenic changes in tropospheric composition increase crop herbivory by insects. Environ Entomol 34:479–485

Hendrey GR, Ellsworth DS, Lewin KF, Nagy J (1999) A free-air enrichment system for exposing tall forest vegetation to elevated atmospheric CO_2. Global Change Biol 5:293–309

Herde O, Pena-Cortes H, Fuss H, Willmitzer L, Fisahn J (1999) Effects of mechanical wounding, current application and heat treatment on chlorophyll fluorescence and pigment composition in tomato plants. Physiol Plantarum 105:179–184

Hoad SP, Marzoli A, Grace J, Jeffree CE (1998) Response of leaf surfaces and gas exchange to wind stress and acid mist in birch (*Betula pubescens*). Trees Struct Funct 13:1–12

Hood IA, Sandberg CJ, Barr CW, Holloway WA, Bradbury PM (1990) Changes in needle retention associated with the spread and establishment of *Phaeocryptopus gaeumannii* in planted Douglas fir. Eur J For Pathol 20:418–429

Horton P, Ruban AV, Walters RG (1996) Regulation of light harvesting in green plants. Annu Rev Plant Phys 47:655–684

Hunter MD (2001) Effects of elevated atmospheric carbon dioxide on insect–plant interactions. Agr For Entomol 3:153–159

Hunter MD, Forkner RE (1999) Hurricane damage influences foliar polyphenolics and subsequent herbivory on surviving trees. Ecology 80:2676–2682

Jiao J, Goodwin P, Grodzinski B (1999) Inhibition of photosynthesis and export in geranium grown at two CO_2 levels and infected with *Xanthomonas campestris* pv Pelargonii. Plant Cell Environ 22:15–25

Jones H (1999) Use of thermography for quantitative studies of spatial and temporal variation of stomatal conductance over leaf surfaces. Plant Cell Environ 22:1043–1055

Jwa NS, Walling LL (2001) Influence of elevated CO_2 concentration on disease development in tomato. New Phytol 149:509–518

Karban R, Myers JH (1989) Induced plant responses to herbivory. Annu Rev Ecol Syst 20:331–348

Karnosky DF et al (2002) Interacting elevated CO2 and tropospheric O3 predisposes aspen (*Populus tremuloides* Michx.) to infection by rust (*Melampsora medusae* f. sp tremuloidae). Glob Change Biol 8:329–338

Kessler A, Baldwin IT (2002) Plant responses to insect herbivory: the emerging molecular analysis. Annu Rev Plant Biol 53:299–328

Knepp RG, Hamilton JG, Mohan JE, Zangerl AR, Berenbaum MR, DeLucia EH (2005) Elevated CO_2 reduces leaf damage by insect herbivores in a forest community. New Phytol 167:207–218

Leon J, Rojo E, Sanchez-Serrano JJ (2001) Wound signaling in plants. J Exp Bot 52:1–9

Lindroth RL, Kinney KK, Platz CL (1993) Responses of deciduous trees to elevated atmospheric CO_2—productivity, phytochemistry, and insect performance. Ecology 74:763–777

Lowman MD (1984) An assessment of techniques for measuring herbivory: is rainforest defoliation more intense than we thought. Biotropica 16:264–268

Luque J, Cohen M, Save R, Biel C, Alvarez IF (1999) Effects of three fungal pathogens on water relations, chlorophyll fluorescence and growth of *Quercus suber* L. Ann For Sci 56:19–26

Macfall JS, Spaine P, Doudrick R, Johnson GA (1994) Alterations in growth and water-transport processes in fusiform rust galls of pine, determined by magnetic-resonance microscopy. Phytopathol 84:288–293

Malmstrom CM, Field CB (1997) Virus-induced differences in the response of oat plants to elevated carbon dioxide. Plant Cell Environ 20:178–188

Manter DK, Kavanagh KL (2003) Stomatal regulation in Douglas fir following a fungal-mediated chronic reduction in leaf area. Trees Struct Funct 17:485–491

Omasa K, Takayama K (2003) Simultaneous measurement of stomatal conductance, non-photochemical quenching, and photochemical yield of Photosystem II in intact leaves by thermal and chlorophyll fluorescence imaging. Plant Cell Physiol 44:1290–1300

Osmond CB, Berry JA, Balachandran S, Buchenosmond C, Daley PF, Hodgson RAJ (1990) Potential consequences of virus infection for shade-sun acclimation in leaves. Bot Acta 103:226–229

Osmond CB, Daley PF, Badger MR, Luttge U (1998) Chlorophyll fluorescence quenching during photosynthetic induction in leaves of *Abutilon striatum* Dicks. infected with *Abutilon* mosaic virus, observed with a field-portable imaging system. Bot Acta 111:390–397

Oxborough K (2004) Imaging of chlorophyll a fluorescence: theoretical and practical aspects of an emerging technique for the monitoring of photosynthetic performance. J Exp Bot 55:1195–1205

Oxborough K (2005) Using chlorophyll a fluorescence imaging to monitor photosynthetic performance. In: Govindjee, Papageorgiou GC (eds) Chlorophyll fluorescence: a signature of photosynthesis. Kluwer, Dordrecht, pp 409–428

Peterson RB, Aylor DE (1995) Chlorophyll fluorescence induction in leaves of *Phaseolus vulgaris* infected with bean rust (*Uromyces appendiculatus*). Plant Physiol 108:163–171

Repka V (2002) Chlorophyll-deficient mutant in oak (*Quercus petraea* L.) displays an accelerated hypersensitive-like cell death and an enhanced resistance to powdery mildew disease. Photosynthetica 40:183–193

Rolfe SA, Scholes JD (1995) Quantitative imaging of chlorophyll fluorescence. New Phytol 131:69–79

Saikkonen K, Ahlholm J, Helander M, Poteri M, Tuominen J (2001) Experimental testing of rust fungus-mediated herbivory resistance in *Betula pendula*. For Pathol 31:321–329

Schenk PM, Kazan K, Wilson I, Anderson JP, Richmond T, Somerville SC, Manners JM (2000) Coordinated plant defense responses in *Arabidopsis* revealed by microarray analysis. Proc Natl Acad Sci USA 97:11655–11660

Scherm H (2004) Climate change: can we predict the impacts on plant pathology and pest management?. Can J Plant Pathol Rev Can Phytopathol 26:267–273

Schlesinger WH, Lichter J (2001) Limited carbon storage in soil and litter of experimental forest plots under increased atmospheric CO_2. Nature 411:466–469

Schulz B, Boyle C, Draeger S, Rommert AK, Krohn K (2002) Endophytic fungi: a source of novel biologically active secondary metabolites. Mycol Res 106:996–1004

Shure DJ, Mooreside PD, Ogle SM (1998) Rainfall effects on plant-herbivore processes in an upland oak forest. Ecology 79:604–617

Singsaas EL, Ort DR, DeLucia EH (2000) Diurnal regulation of photosynthesis in understory saplings. New Phytol 145:39–49

Smith WK, Brodersen CR, Hancock TE, Johnson DM (2004) Integrated plant temperature measurement using heat-sensitive paint and colour image analysis. Funct Ecol 18:148–153

Stiling P, Cattell M, Moon D, Rossi A, Hungate BA, Hymus GM, Drakes B (2002) Elevated atmospheric CO_2 lowers herbivore abundance, but increases leaf abscission rates. Global Change Biol 8:658–667

Swain PH, Davis SM (eds) (1978) Remote sensing: the quantitative approach. McGraw-Hill, New York

Tang JY, Zielinski RE, Zangerl AR, Crofts AR, Berenbaum MR, DeLucia EH (2006) The differential effects of herbivory by first and fourth instars of *Trichoplusia ni* (Lepidoptera: Noctuidae) on photosynthesis in *Arabidopsis thaliana*. J Exp Bot 57:527–536

Thordal-Christensen H, Zhang Z, Wei Y, Collinge DB (1997) Subcellular localization of H_2O_2 in plants. H_2O_2 accumulation in papillae and hypersensitive response during the barley-powdery mildew interaction. Plant J 11:1187–1194

Welter SC (1989) Arthropod impact on plant gas exchange. In: Bernays EA (eds) Insect–plant interactions. CRC Press, Boca Raton, pp 135–151

Zangerl AR, Hamilton JG, Miller TJ, Crofts AR, Oxborough K, Berenbaum MR, DeLucia EH (2002) Impact of folivory on photosynthesis is greater than the sum of its holes. Proc Natl Acad Sci USA 99:1088–1091